AIAA JOURNAL
Vol. 31, No. 12, December 1993

Hypersonic Crossing Shock-Wave/Turbulent-Boundary-Layer Interactions

M. I. Kussoy* and K. C. Horstman†
Eloret Institute, Palo Alto, California 94303
and
C. C. Horstman‡
NASA Ames Research Center, Moffett Field, California 94035

Experimental data for two three-dimensional intersecting shock-wave/turbulent-boundary-layer interaction flows at Mach 8.3 are presented. The test bodies, composed of two sharp fins fastened to a flat plate test bed, were designed to generate flows with varying degrees of pressure gradient, boundary-layer separation, and turning angle. The data include surface pressure and heat transfer distributions as well as mean flowfield surveys both in the undisturbed and interaction regimes. The persistence of an extensive low-pressure region throughout the flowfield demonstrates that a sidewall compression inlet is not an efficient pressure increasing device. The data have been obtained in sufficient detail to validate existing or future computational models of these hypersonic flows.

Nomenclature

P = pressure
$PT2$ = pitot pressure
Q = heat flux
T = temperature
x, X = streamwise coordinate, distance from leading edge of sharp fin
y, Y = distance normal to flat plate model surface
z, Z = spanwise distance measured from symmetry line of test geometry
α = yaw or fin angle

Subscripts
w = wall
0 = stagnation conditions
∞ = local freestream ahead of interaction

Introduction

TO design aerodynamic vehicles to fly in the hypersonic flow regime, it is of primary importance to have the ability to predict, with reasonable reliability, their aerodynamic characteristics. Only in this manner can long and expensive design programs be successful as efficient designs are identified and studied. However, before one attempts to predict the aerodynamics of the flow over a complex vehicle, one must first be able to reliably predict basic flow properties on simple generic shapes. Without verification of computations through experimental measurements on a simple body, any a priori prediction of the flowfield over a complex body could be in gross error.

One of the key elements in any airbreathing hypersonic vehicle is the inlet. This device, usually composed of two or more vertical surfaces attached to the vehicle's surface and covered by a cowl, is normally located in a far downstream position at the end of a ramp. We have identified several key elements of a generic hypersonic inlet: a thick turbulent boundary layer approaching two vertical fins, a crossing shock pattern, vortices, large pressure gradients, and separation zones. An experiment was designed that focused on these salient features of a generic hypersonic inlet. The basic configuration consisted of a pair of sharp vertical fins attached to a flat plate test bed. The approaching undisturbed equilibrium fully developed hypersonic turbulent boundary layer (which was verified by detailed boundary-layer surveys) occupied 20% of the open inlet area. The fin-spacing geometry was determined as that which would allow the two primary shocks to intersect without any weakening from the expansion fans originating from the downstream inside corners of the fins.

Two pairs of fins, with compression angles of 10 and 15 deg, respectively, were tested to observe the effect of different shock strengths on the entire flowfield. This paper presents experimental data obtained using these test models. The data obtained during this test program can be used for verifying computer codes. These data will significantly add to the meager hypersonic database.[1] Turbulence models can then be evaluated against relatively simple three-dimensional flows, which is a first step for the development of models for the more complex flow over a real vehicle.

Description of Experiment

The following section will only include a brief description of this experimental investigation. Complete details of the test models, instrumentation, and data reduction techniques employed can be found in Ref. 2.

Facility

The experiment was conducted in the NASA Ames 3.5-ft hypersonic wind-tunnel facility where heated high-pressure air flows through a 1.067-m diam test section to four low-pressure spheres. The tunnel is of the open jet design, which allows models to remain outside the stream until the required flow conditions are established. Models are rapidly inserted into the stream and just as rapidly retracted before tunnel shutdown. Damage to models and instrumentation is thus minimized. The freestream test core diameter was approximately 0.6 m. Useful test time was 3 min. Run-to-run variations in tunnel pressure were less than 0.5%. However, the wind-tunnel total temperature varied up to 50 K from run to run and, in addition, during a single run it varied about 90 K over the 3-min test time. These variations required special heat transfer data reduction procedures, which are discussed in Ref. 2.

Received Oct. 1, 1992; revision received Jan. 8, 1993; accepted for publication Jan. 9, 1993; presented as Paper 93-0781 at the AIAA 31st Aerospace Sciences Meeting, Reno, NV, Jan. 11–14, 1993.

*Principal Investigator, 3788 Fabian Way. Member AIAA.
†Research Scientist, 3788 Fabian Way; currently Research Engineer, General Electric Co., 175 Curtner Avenue, San Jose, CA 95125.
‡Senior Scientist, Fluid Dynamics Division. Associate Fellow AIAA.

Test Models

The test bed consisted of a sharp flat plate, 76 cm wide, 220 cm long, and 10 cm thick (Fig. 1). The plate was pitched at a −2-deg angle of attack to increase the test Reynolds number and provide a uniform two-dimensional flowfield on the plate. The turbulent boundary-layer thickness at the downstream end of the test bed was approximately 4 cm. The leading edge of the plate consisted of a 10-deg invar wedge. The bed was of a hollow frame construction, with interchangeable access panels (76 cm wide, 25.4 cm long, and 0.6 cm thick) covering the upper and lower surfaces. The entire test bed was water cooled, maintaining a constant surface temperature of 300 ± 5 K during a run. (Cooling was turned off during the heat transfer runs.) Several of the interchangeable access panels had 20-cm diam holes in the center that would accommodate several different instrumentation ports. One port was instrumented with a series of pressure taps and two types of heat transfer gauges. Another port, uninstrumented, accommodated a computer-controlled survey mechanism to which static pressure, total pressure, flow direction (yaw), and total temperature probes could be attached for flowfield surveys.

The fin pairs were placed on the test bed as shown in Fig. 1. Two geometries were tested: one pair had compression angles of 10 deg and the other 15 deg. The separation between the vertical sides was 15.2 cm at the fin leading edge and 4.3 cm in the channel at the rear. These dimensions remained constant for the entire test series. The fin pairs could easily move between runs in the x or z direction by means of slotted brackets attached to the fins and a slotted piece attached to the flat plate surface. Thus, continuous data were obtained throughout the interaction region by moving the fin pair for each run in either the x or z direction while the instrumentation port remain fixed.

Instrumentation

One instrumented port was used in this investigation. This port, used on the test bed, was 20 cm in diameter and had rows of parallel pressure taps, thermocouples, and Schmidt-Boelter heat transfer gauges that ran close to and on either side of the centerline. This port had a series of mounting holes along the edge and could be oriented in any direction with respect to the oncoming undisturbed flow. Complete details are included in Ref. 2.

The surface static pressure taps were 0.16 cm in diameter, connected with short lengths of stainless steel tubing (10–15 cm long) to individual strain gauge differential-pressure transducers (PSI brand). These pressure cells were all located in a small self-contained modular unit, which had a built-in pressure scanning system (electrical, not mechanical). This system was designed to be calibrated in situ with carefully monitored pressures. The calibrations were made by varying the pressure on the reference side of the cell and recording it using a Datametric strain-gauge differential pressure cell that itself had been calibrated previously with a deadweight tester. Calibrations were made immediately before each run and were linear and repeatable to within 1%. The modular unit containing the transducers was located within the test bed and was water cooled.

Surface heat transfer was obtained using two techniques: the transient thin-skin method and a measurement using a thermopile. The transient thin-skin method used chromel-constantan thermocouples spot welded approximately 1 cm apart to the interior surface of the instrumentation ports. The port thickness was approximately 0.25 cm. For these tests, the entire model was kept at room temperature and then inserted into the flow after the desired flow conditions were obtained. Depending on the thermocouple location, the temperature rise (with the internal model water cooling disconnected) varied from 10 to 70 K during a typical 5- to 10-s heat transfer run.

Heat transfer rates were also measured using miniature Schmidt-Boelter heat transfer gauges. These gauges, 0.2 cm in diameter by 0.6 cm long, consisted of a thermopile to measure the temperature difference across a known substrate located just below the surface. A factory calibration was used to relate the gauge output to the heat transfer rate q. These gauges are essentially steady-state devices, giving a stable reading after about a second or two.

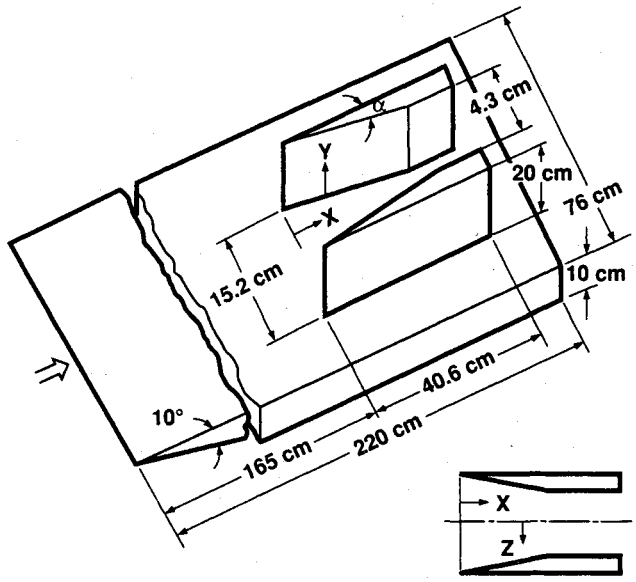

Fig. 1 Test body configuration and coordinate system.

They were placed 1.8 cm apart. Although the data reduction procedure for the Schmidt-Boelter gauges is simpler than the thin-skin method, the results from the thin-skin method are more consistent and believed to be more reliable than the results from the Schmidt-Boelter gauges. The results plotted in this article are from the thin-skin method.

Flowfield surveys were obtained with a computer-controlled survey mechanism located within the model. This mechanism was designed to move a probe in two directions—vertical (Y) and yaw (α)—using individual motors. Pitot and static pressure and total temperature were measured ahead of the interaction using single probes. See Ref. 2 for detailed descriptions of these probes and the data reduction and correction procedures used.

To measure pitot pressure and yaw angle in the interacting flowfield, a three-hole flow direction probe (cobra probe) was used. The diameters of the individual tubes were 0.107 cm, and the overall width was three times that, or 0.32 cm. The probe was calibrated in the undisturbed boundary layer at several vertical positions (thus varying Mach number) for a range of yaw angles. The calibration provided us with the zero offset, wall interference effects, as well as the usable Mach number and yaw angle range. The results of these calibrations showed that the probe calibration was independent of Mach number and usable for $y > 0.2$ cm and up to yaw angles of 25 deg (the maximum yaw angle measured in these flows). With this technique the procedure was to fix the probe yaw angle and incrementally raise the probe through the boundary layer.

Experimental Uncertainties

The experimental uncertainties listed later were determined from run-to-run measurement scatter, comparisons of different measurement techniques, and instrumentation accuracy. The uncertainties in the surface pressure are estimated to be ±10% or ±80 N/m^2, whichever is larger. The uncertainties in surface heat flux measurements are estimated to be ±10%. For the flowfield quantities, the estimated uncertainties are ±2% for the total temperature, ±10% for the static pressure, ±6% for the static temperature, ±12% for the density, ±3% for the velocity, ±3 deg for yaw angle, and ±5% for the pitot pressure. The uncertainty in Y is ±0.02 cm. These uncertainties in the flowfield variables are due principally to zero offsets in the pressure and yaw angle measurements.

Results and Discussion

An important objective of this work was to provide a well-documented experimental database for validating computational models. The data are presented in tabular form in Ref. 2.

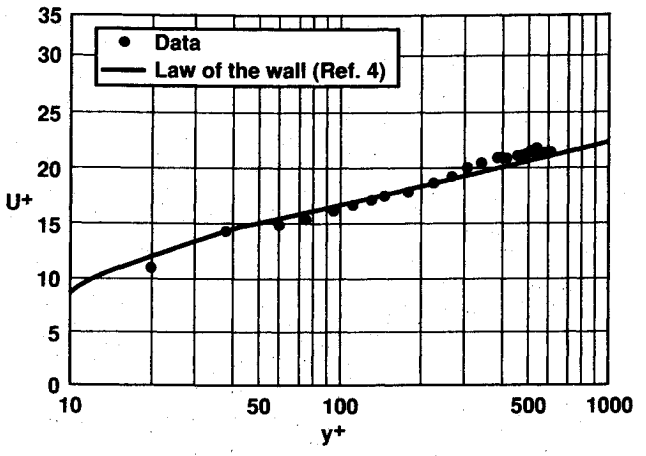

Fig. 2 Mean velocity distribution in law-of-the-wall coordinates for the undisturbed boundary layer.

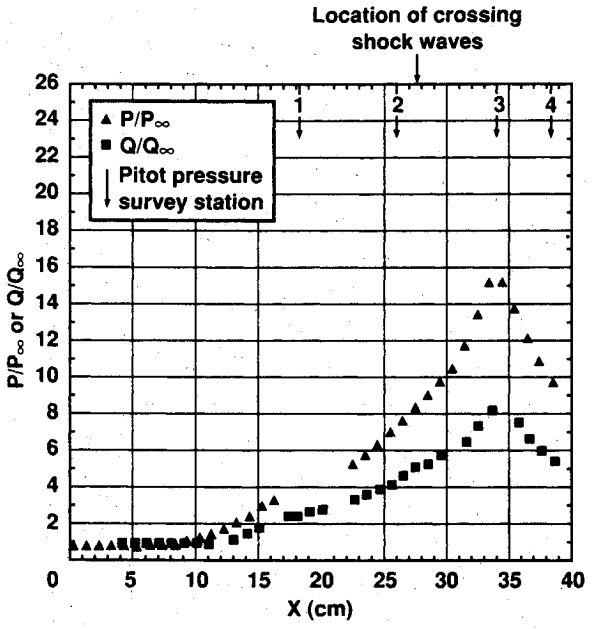

Fig. 3 Streamwise variation of pressure and heat transfer on the flat plate surface ($y, z = 0$ cm), 10-deg double fin configuration.

Undisturbed Test Bed Results

To determine whether a fully developed, hypersonic, turbulent boundary layer exists ahead of the interaction region, boundary-layer surveys were made at 162 cm downstream of the flat plate leading edge using a pitot probe, a static-pressure probe, and a total-temperature probe. The measured local freestream test conditions were wall temperature ratio $T_w/T_0 = 0.27$, freestream unit Reynolds number $= 5.3 \times 10^6$/m, and freestream Mach number $= 8.3$. These surveys are fully described in Ref. 2. The velocity profiles obtained from these mean flowfield surveys were transformed into incompressible coordinates using the Van Driest transformation[3] and are shown in Fig. 2 in law-of-the-wall coordinates. Also shown on this plot is Coles' universal law of the wall.[4] These profiles verify the presence of a hypersonic equilibrium turbulent boundary layer ahead of the interaction region for the fin flows being investigated. The skin-friction coefficient determined from a Clauser plot is 0.99×10^{-3}. The incoming boundary layer has a thickness of 3.25 cm, a momentum thickness of 0.083 cm, and a momentum thickness Reynolds number of 4.4×10^3. In this investigation, $T_w/T_0 = 0.27$; thus the boundary layer has a strong driving potential for easy measurement of the heat transfer. All measurements were made within the region bounded by the shock wave from the flat plate leading edge (inclined at -2 deg) and the flat plate surface itself.

The flat plate instrumentation port was aligned with its rows of instrumentation parallel to the incoming flow direction and measurements were made from the most downstream to the most upstream positions on the flat plate that were physically possible (80–180 cm from the leading edge). The resulting longitudinal pressure and heat transfer distributions are reported in Ref. 5. The pressure was essentially constant, whereas the heat transfer decreased as x increased between 100 and 180 cm from the leading edge. It is speculated that the end of natural transition occurred at about 100 cm (where a maximum value of heat transfer was measured), although we have no direct measurements throughout the transition region.

The flat plate instrumentation port was also oriented perpendicular to the incoming flow. Measurements indicated that both pressures and heat transfer rates were essentially constant over an 18-cm-wide, centrally located zone on the model surface both 165 and 190 cm back from the leading edge. (Variations in these data in this zone were within the experimental accuracy of the measurements.) Also, results from surface oil film studies showed a 50-cm-wide area of surface skin-friction lines parallel to the flat plate centerline and provided an indication of the two dimensionality of the incoming flow. From the foregoing results it was concluded that a two-dimensional boundary layer existed, running parallel to the plate edges, with negligible streamwise gradients, and it became quite thick (nearly 4 cm) at the rearward stations where the interactive flow was initiated.

Double Fin Interaction Results

The flat plate instrumentation port was positioned, in separate runs, with either the row of pressure taps or thermocouples on the plane of symmetry. The resulting pressure and heat transfer distributions are shown in Figs. 3 and 4 for the 10- and 15-deg double fins, respectively. The data are normalized by the measured undisturbed values forward of the interaction. The location of the intersection of the inviscid shock waves is noted for each configuration. Also noted are the axial locations chosen for the pitot pressure and yaw angle profiles. For each case the pressure rises rapidly to a maximum value located downstream of the shock crossing loca-

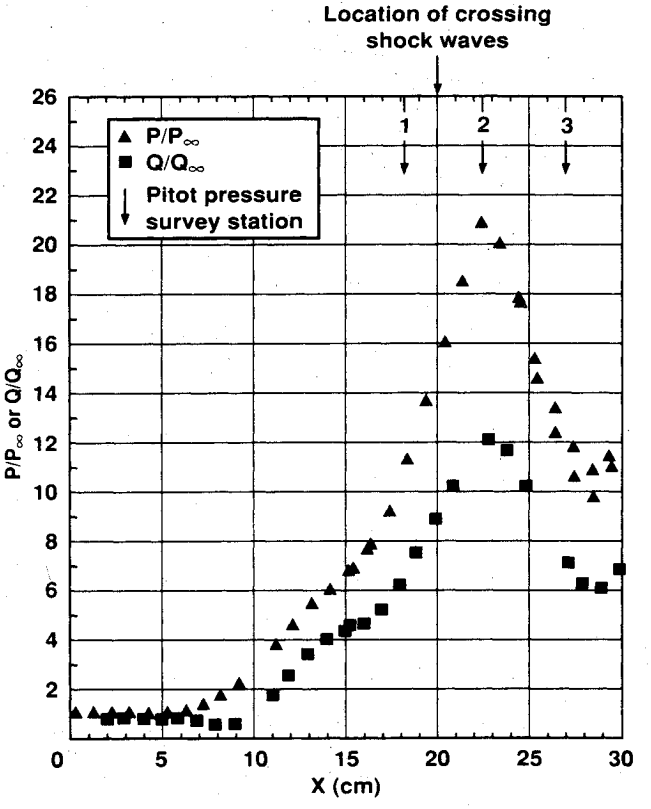

Fig. 4 Streamwise variation of pressure and heat transfer on the flat plate surface ($y, z = 0$ cm), 15-deg double fin configuration.

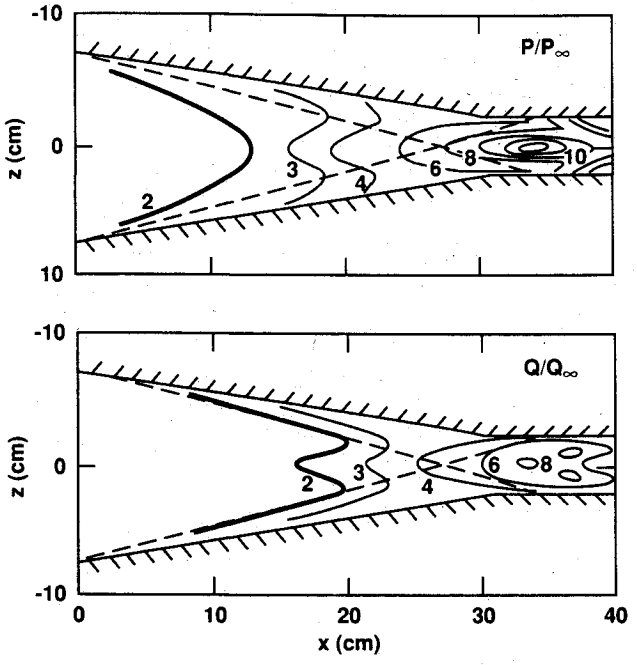

Fig. 5 Surface contours of pressure and heat transfer for the 10-deg double fin configuration.

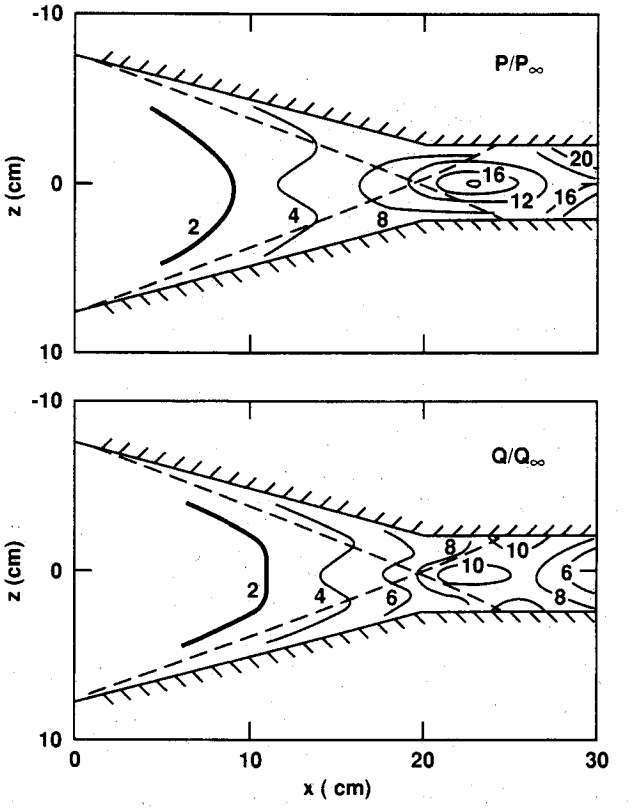

Fig. 6 Surface contours of pressure and heat transfer for the 15-deg double fin configuration.

tion. This is followed by a decrease caused by the expansion fan originating from the interior corners of the fins. The maximum values fall well below the inviscid values, $P/P_\infty = 30.5$ and 45.4 for the 10- and 15-deg cases, respectively. The normalized heat transfer data fall below the pressure results and exhibit peak values at the same x locations as the pressure peaks. The heat transfer data show a small plateau near the initial rise for both configurations.

In addition to measurements along the centerline, the instrumentation port was positioned in the transverse direction at several axial locations for each geometry. Contour plots of surface pressure and heat transfer data are shown in Figs. 5 and 6 for the 10- and 15-deg cases, respectively. These plots are only approximate because of the lack of detailed data in the axial direction off centerline. (Transverse pressure data were obtained at four axial locations and heat transfer data at eight locations.) The dashed line indicates the location of the inviscid shock waves. For both cases, the pressure and heat transfer results display narrow spanwise peaks at the centerline located slightly downstream of the inviscid crossing shock location. A distinct second heat transfer peak near the wall is noted for the 15-deg case. This is where the crossing

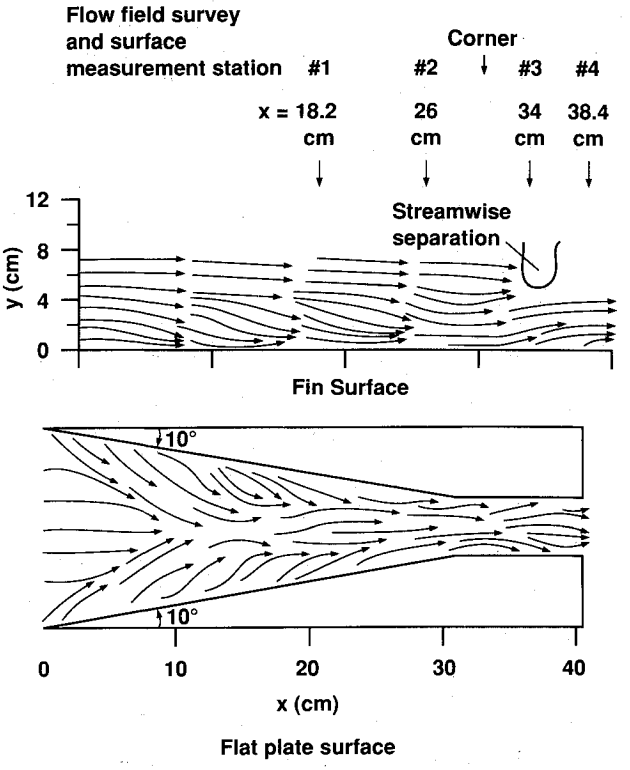

Fig. 7 Surface flow visualization, 10-deg double fin configuration.

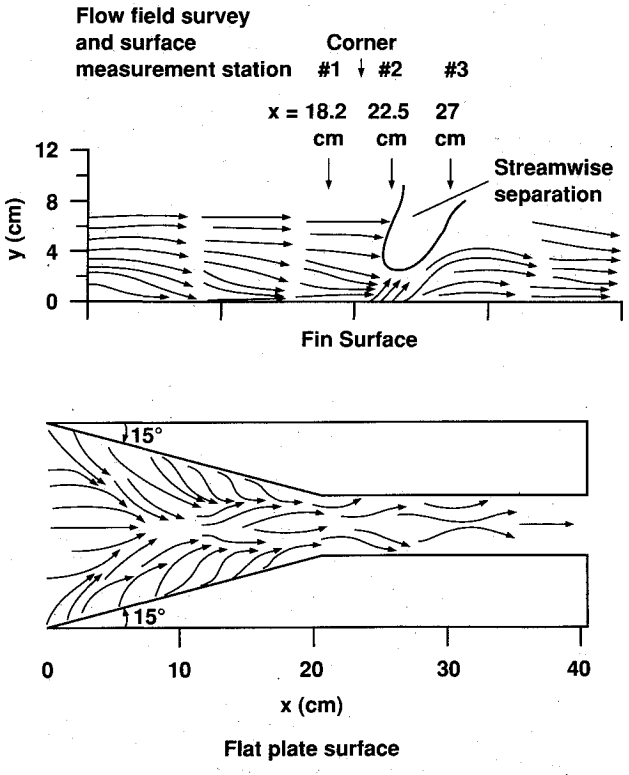

Fig. 8 Surface flow visualization, 15-deg double fin configuration.

shocks intersect the wall. No strong peak near the wall was found for the 10-deg case.

Oil flow visualizations were made for each fin configuration on both the flat plate and fin surfaces, using a thin mixture of machine oil and chalk dust. The oil would burn off or flow downstream, leaving a thin trace of chalk dust on the surface, which could be lifted off (using 20-cm-wide scotch tape) and permanently placed on a plain white sheet of paper. Since the originals do not reproduce well, flow directions were traced from the original data and are shown in Figs. 7 and 8. For convenience, the transverse measuring stations are shown in these figures. Both fin geometries show similar features. On the flat plate surface, two three-dimensional separation lines originate at the fin leading edges and come close to merging at the centerline. It was impossible to tell whether or not an actual merging took place. Moving downstream, the skin-friction lines diverge and then converge again forming a "coke bottle" pattern. This pattern is likely due to the two counter-rotating vortices merging at the centerline of this flowfield. On the fin surfaces near the leading edge and $y=0$, the downward turning of the skin-friction lines suggests the presence of corner vortices. Downstream, for $y>4$ cm, streamwise separation is noted at a location where the shock wave intersects the wall. (The fin boundary layer is either laminar or transitional at these locations, thus making it easier to separate the flow as opposed to a turbulent boundary layer.) For the 15-deg case there is a sharp upturning of the flow below the streamwise separation zone.

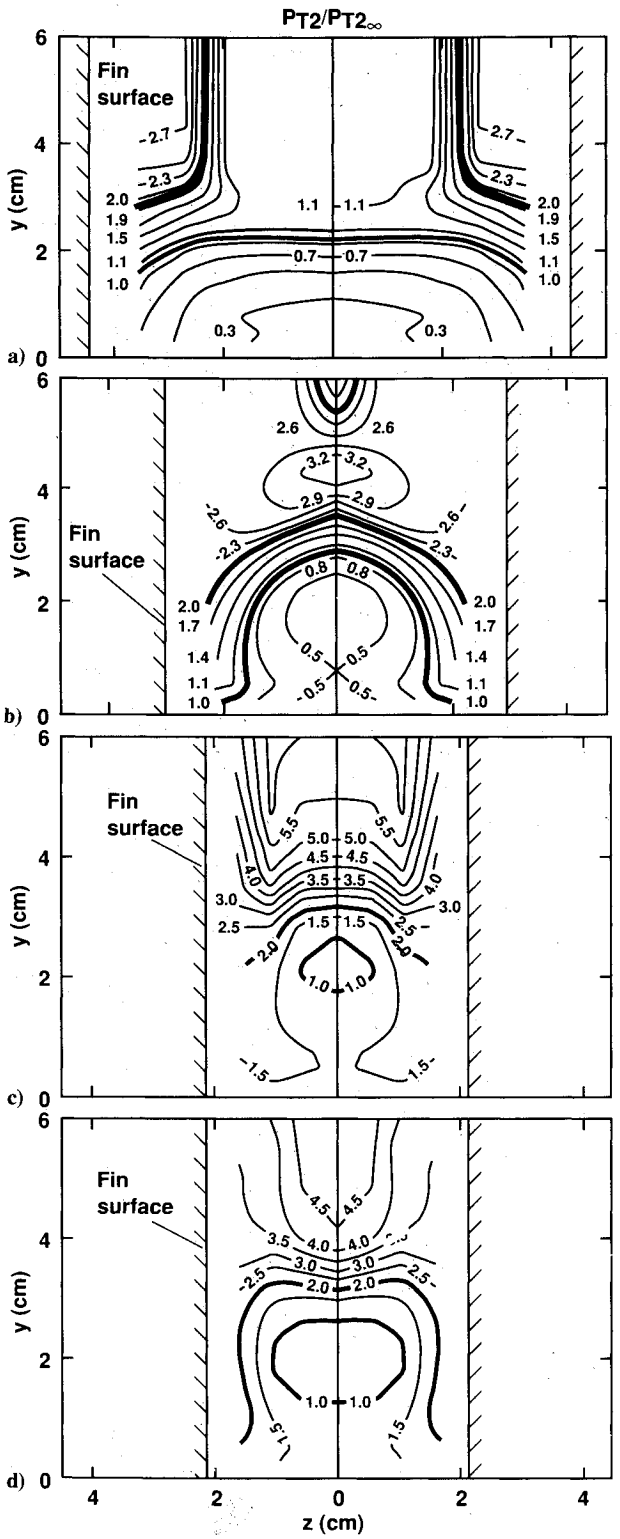

Fig. 9 Flowfield pitot pressure contours for the 10-deg double fin configuration: a) station 1, $x=18.2$ cm; b) station 2, $x=26.0$ cm; c) station 3, $x=34.0$ cm; and d) station 4, $x=38.3$ cm.

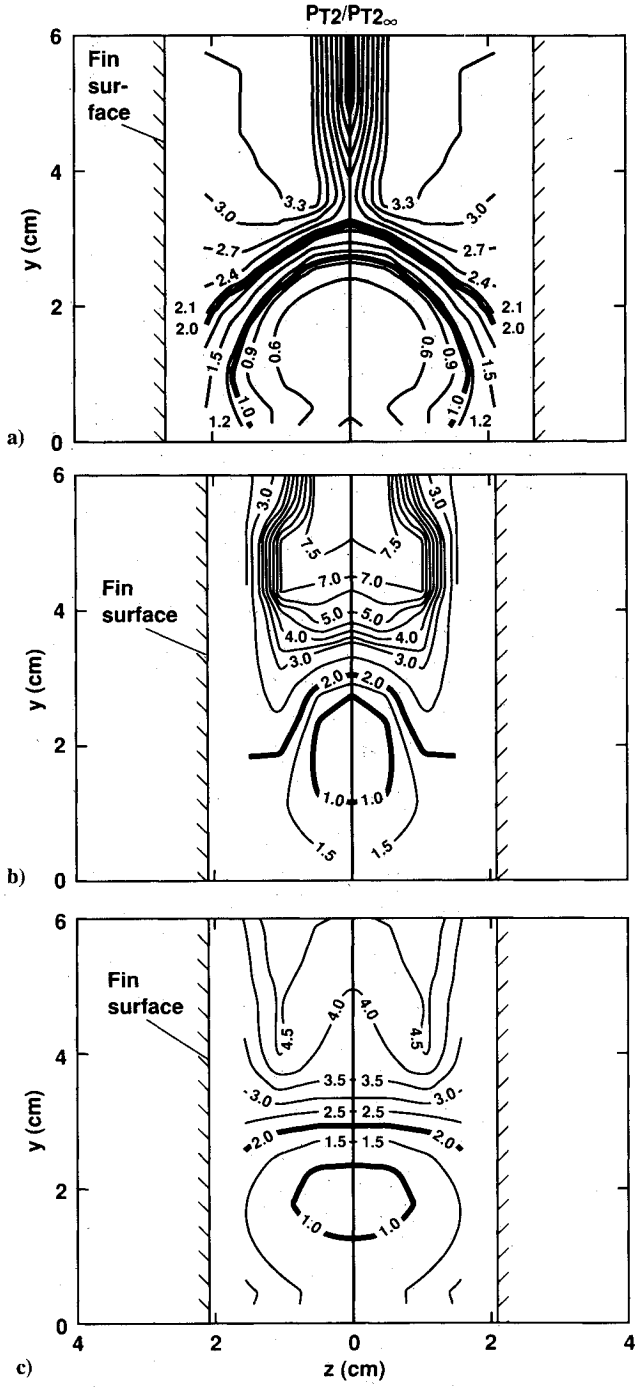

Fig. 10 Flowfield pitot pressure contours for the 15-deg double fin configuration: a) station 1, $x=18.2$ cm; b) station 2, $x=22.5$ cm; and c) station 3, $x=27.0$ cm.

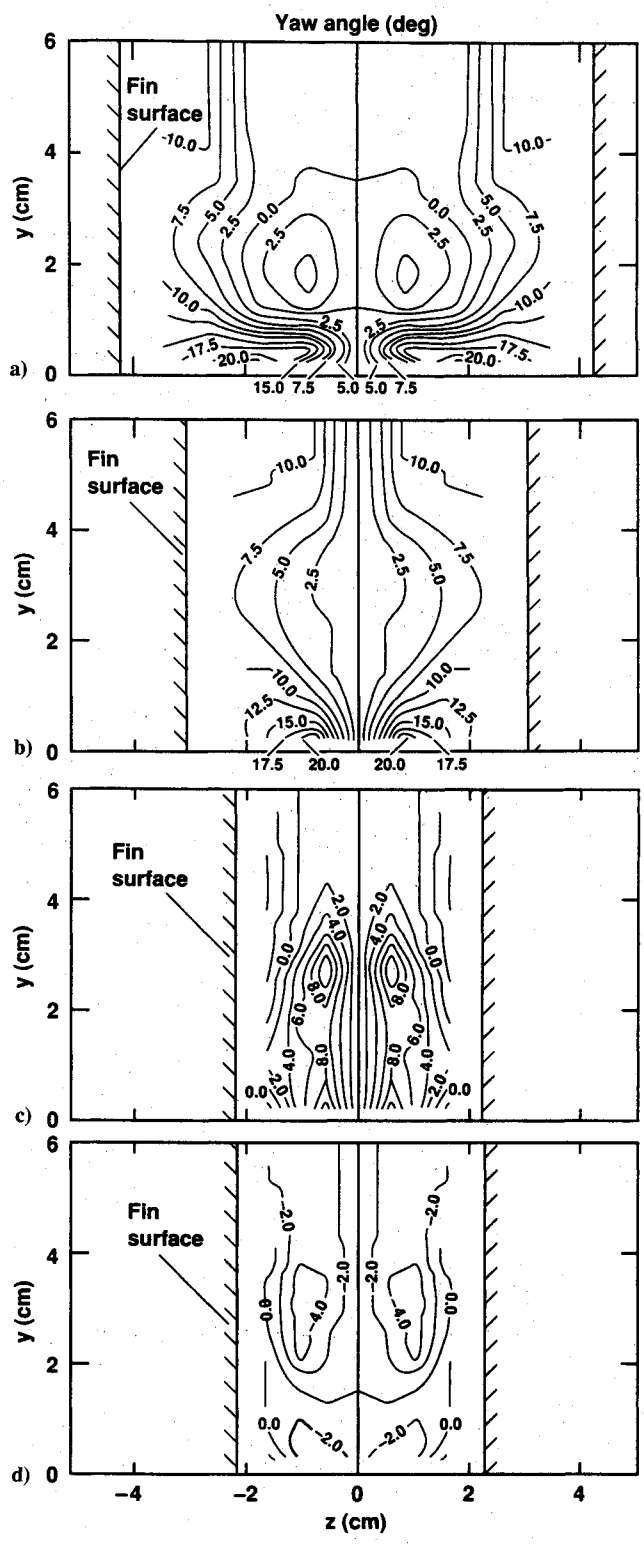

Fig. 11 Flowfield yaw angle contours for the 10-deg double fin configuration: a) station 1, $x = 18.2$ cm; b) station 2, $x = 26.0$ cm; c) station 3, $x = 34.0$ cm; and d) station 4, $x = 38.3$ cm.

Two sets of flowfield surveys were done, one for each of the configurations investigated. For both configurations, at each transverse station, the distance between the centerline ($z = 0$) and the fin surface was divided into four or five equal increments, and surveys were made in the y direction, at each of these equally spaced z increments. In the converging part of the geometry, the cobra probe axis was set to the fin angle (10 or 15 deg), and in the channel part, it was set to point directly upstream. It was felt that fixing the probe at these angles would ensure that it would always be operating within its valid calibration range. Pitch was not measured, but it was felt that pitch angles of less than 10 deg (which would seem to be the case here) would not affect the yaw results. These data were processed to give contour plots in the y-z plane.

Normalized pitot pressure contours are shown for several x locations for the 10-deg fin configuration in Fig. 9 and for 15-deg in Fig. 10. Describing the 10-deg results, in Fig. 9a (station 1, $x = 18.2$ cm) the incoming boundary layer is discerned, and it is evident that it takes up a substantial portion of the surveyed flowfield. The two shocks, indicated by the closely paired vertical contours, are also distinctly seen. Moving downstream to station 2 (Fig. 9b), the inviscid shock waves have intersected. The low-pressure region, arbitrarily indicated by the bold $PT2/PT2_\infty = 2$ contour line, occupies approximately half the surveyed area. The portion of the flow with a pitot pressure ratio less than 1 has actually increased in height and occupies a larger percentage of the flowfield. There is also a higher pressure region forming at about $y = 4$

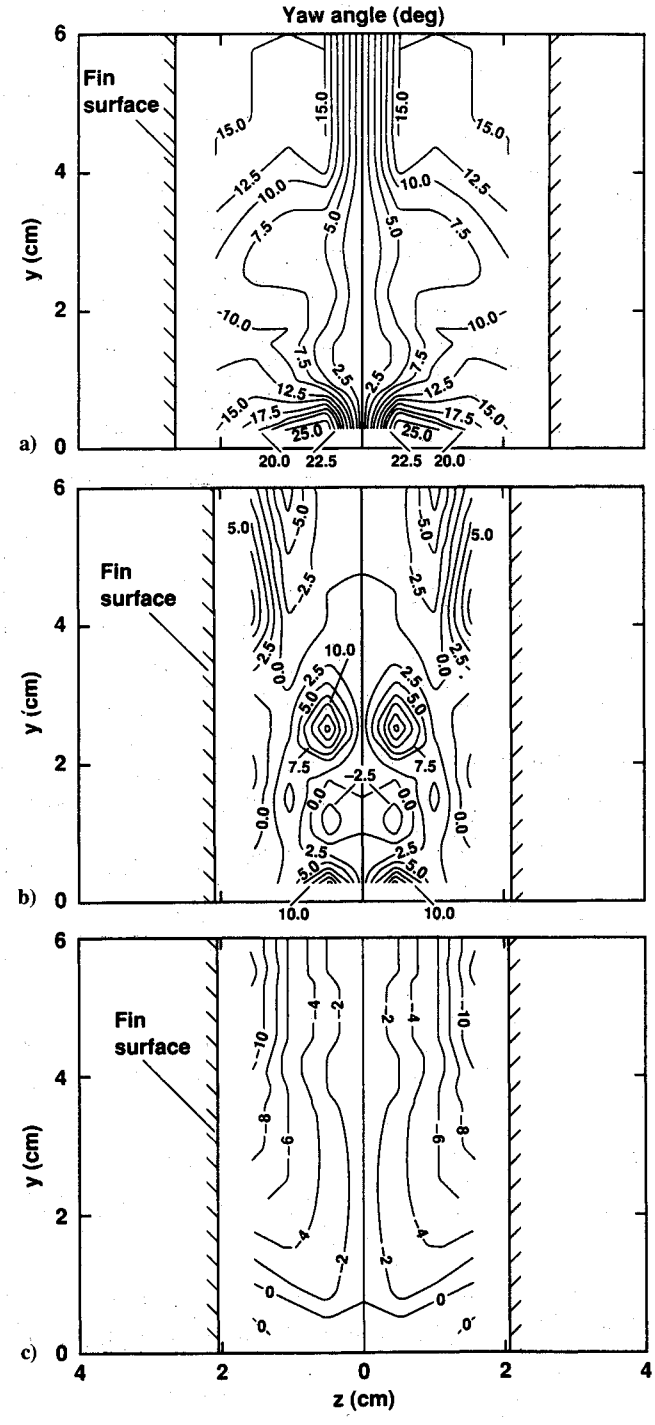

Fig. 12 Flowfield yaw angle contours for the 15-deg double fin configuration: a) station 1, $x = 18.2$ cm; b) station 2, $x = 22.5$ cm; and c) station 3, $x = 27.0$ cm.

cm. These first two stations were in the converging part of the channel formed by the fins. The next two stations were in the straight section of the channel. For stations 3 and 4 (Figs. 9c and 9d) it is seen that the low pressure portion of the flow does not disappear or even diminish but remains essentially the same in extent, taking up about half of the channel at these last two measuring stations. The highest pressure ratios measured in the straight channel, 5.5 to 6, agree with inviscid calculations.

The results for the 15-deg fin configuration (Fig. 10) show similar trends. The pitot pressure contours shown in Figs. 10a–10c are at the same relative locations to the inviscid shock intersertion as the data shown in Figs. 9b–9d. In Fig. 10a the intersection shocks are stronger and penetrate deeper toward the flat plate surface. After the intersection, Fig. 10b, the shocks are much stronger and well defined. Otherwise the basic flow structure is quite similar for the two test cases.

Normalized yaw angle contours are shown for several x locations for the 10-deg fin configuration in Fig. 11 and for 15-deg in Fig. 12. Describing the 10-deg results, in Fig. 11a (station 1, $x = 18.2$ cm) a very large turning exists near the plate surface. This is a result of the large counter-rotating vortices formed by the upstream interaction of the sharp fin generated shock wave with the boundary layer. The two inviscid shocks, indicated by the closely paired vertical contours, are also distinctly seen. Moving downstream to station 2 (Fig. 11b), the inviscid shock waves have intersected. The large yaw angles are still present near the plate surface. At the next station (Fig. 11c), the large turning angles near the surface have vanished. A significant flow structure has appeared near the centerline at $y = 3$ cm (evidenced by the peaks in yaw angle). The pitot pressure contours show no evidence of this structure. Further measurements using optical techniques will be required to resolve and understand this flow feature. At the last station (Fig. 11d), the yaw angle is small throughout most of the flowfield.

The results for the 15-deg fin configuration (Fig. 12) show similar trends. Again, to compare the two fin angles, Figs. 12a–12c should be compared with Figs. 11b–11d. Only a few differences are noted. In Fig. 12a the turning near the plate surface is larger, suggesting a stronger vortex. In Fig. 12b the same structure at $y = 3$ cm is observed but with larger values of yaw angle. Finally, at the last station the yaw angles near the fin wall are quite large. This is due to the shock waves reflecting off the fin surfaces near this location.

Concluding Remarks

Two cases of an intersecting shock-wave/hypersonic turbulent boundary-layer interaction flow have been experimentally investigated. These particular cases were chosen because they were relatively simple yet exhibited the same basic characteristics present on generic inlets that would be present on complex hypersonic vehicles. Streamwise and transverse surface pressure and heat transfer distributions, as well as flowfield surveys that measured pitot pressures and yaw angles in the interaction regime, are presented. The tabulated results presented in Ref. 2 provide, in sufficient detail, experimental data for validating present or future turbulence models and computer codes. One important result deserves special attention: the persistence of an extensive low-pressure region far downstream of the fin leading edges. The persistence of this low-pressure region suggests that the generic hypersonic inlet tested here, in which a thick turbulent boundary layer approaches two vertical compression surfaces, would not be a particularly efficient pressure increasing device.

Acknowledgments

The first two authors were supported by a grant from NASA to Eloret Institute (NCC2-452). The authors owe a large debt of gratitude to the personnel at the NASA Ames Research Center's 3.5-ft hypersonic wind tunnel, namely, mechanical test technicians Mike Reeves (shift leader), Robert Finnie, and Reuben Torrecampo and electronic technician Bong de la Cruz. Without their hard work and efforts during this investigation, the present results, obtained during a relatively short tunnel entry, would not have been possible.

References

[1]Settles, G. S., and Dodson, L. J., "Hypersonic Shock/Boundary Layer Interaction Database," AIAA Paper 91-1763, July 1991; see also NASA CR 177577, April 1991.

[2]Kussoy, M. I., and Horstman, K. C., "Intersecting Shock-Wave/Turbulent Boundary-Layer Interactions at Mach 8.3," NASA TM 103909, Feb. 1992.

[3]Van Driest, E. R., "The Problems of Aerodynamic Heating," *Aeronautical Engineering Review*, Vol. 15, No. 10, 1956, pp. 26–41.

[4]Coles, D. E., "The Turbulent Boundary Layer in a Compressible Fluid," Rand Corp., Rept. R-403-PR, Santa Monica, CA, Sept. 1962.

[5]Kussoy, M. I., and Horstman, K. C., "Documentation of Two- and Three-Dimensional Shock-Wave/Turbulent-Boundary-Layer Interaction Flows at Mach 8.2," NASA TM 103838, May 1991.